THE JOURNAL OF BIOLOGICAL CHEMISTRY
Vol. 276, No. 45, Issue of November 9, pp. 42287–42292, 2001

Printed in U.S.A.

F-ATPase: Forced Full Rotation of the Rotor Despite Covalent Cross-link with the Stator*

Received for publication, July 20, 2001, August 27, 2001
Published, JBC Papers in Press, August 31, 2001, DOI 10.1074/jbc.M106884200

Karin Gumbiowski, Dimitri Cherepanov, Martin Müller, Oliver Pänke, Parichart Promto, Stephanie Winkler, Wolfgang Junge, and Siegfried Engelbrecht‡

From the Universität Osnabrück, FB Biologie, Abt. Biophysik, Barbarastrasse 11, 49069 Osnabrück, Germany

In ATP synthase (F_OF_1-ATPase) ion flow through the membrane-intrinsic portion, F_O, drives the central "rotor", subunits $c_{10}\epsilon\gamma$, relative to the "stator" $ab_2\delta(\alpha\beta)_3$. This converts ADP and P_i into ATP. Vice versa, ATP hydrolysis drives the rotation backwards. Covalent cross-links between rotor and stator subunits have been shown to inhibit these activities. Aiming at the rotary compliance of subunit γ we introduced disulfide bridges between γ (rotor) and α or β (stator). We engineered cysteine residues into positions located roughly at the "top," "center," and "bottom" parts of the coiled-coil portion of γ and suitable residues on α or β. This part of γ is located at the center of the $(\alpha\beta)_3$ domain with its C-terminal part at the top of F_1 and the bottom part close to the F_O complex. Disulfide bridge formation under oxidizing conditions was quantitative as shown by SDS-polyacrylamide gel electrophoresis and immunoblotting. As expected both the ATPase activities and the yield of rotating subunits γ dropped to zero when the cross-link was formed at the center (γL262C ↔ αA334C) and bottom (γCys^{87} ↔ βD380C) positions. But much to our surprise disulfide bridging impaired neither ATP hydrolysis activity nor the full rotation of γ and the enzyme-generated torque of oxidized F_1, which had been engineered at the top position (γA285C ↔ αP280C). Apparently the high torque of this rotary engine uncoiled the α-helix and forced amino acids at the C-terminal portion of γ into full rotation around their dihedral (Ramachandran) angles. This conclusion was supported by molecular dynamics simulations: If γCys^{285}-Val^{286} are attached covalently to $(\alpha\beta)_3$ and γAla^{1}-Ser^{281} is forced to rotate, γGly^{282}-Ala^{284} can serve as cardan shaft.

ATP synthases of bacteria, chloroplasts, and mitochondria utilize ion-motive force for the synthesis of ATP from ADP and phosphate (1–3). When operating in reverse (F-ATPase) the enzyme hydrolyzes ATP and generates ion-motive force. The ATP synthase, in its simplest bacterial form, consists of eight different subunits, five in the F_1 portion, $(\alpha\beta)_3\gamma\delta\epsilon$, and three in the F_o portion, $\mathbf{ab_2c}_{10}$ (4). The former subunits catalyze substrate conversion and the latter are responsible for ion translocation. ATP hydrolysis by both isolated F_1 (5–11) and membrane-bound F_1 (12) drives the rotation of $\gamma(\epsilon)$ relative to the $(\alpha\beta)_3$ barrel. The counterpart of these rotor elements in F_1 is the **c**-ring in F_o (13–15). Subunits $\mathbf{a}$–$\mathbf{b}_2$–δ-$(\alpha\beta)_3$ therefore form the stator, and subunits $\mathbf{c}_{10}$–γ-ϵ form the rotor (15, 16).

Mechanistically, the tight coupling between subunits c_{10} and $\gamma\epsilon$ poses the question how the symmetry "mismatch" between the presumed stepwise rotation of the proteolipid oligomer (36° per step) and $\gamma\epsilon$ (120° per step) is overcome. An elastic power transmission between F_O and F_1 has been shown (17, 18). Aiming at the internal elasticity of subunit γ, we introduced disulfide bridges at three different positions along the region where γ passes through the $(\alpha\beta)_3$ cylinder ("top," "center," and "bottom," *cf.* Fig. 1). By introducing a cross-link between the penultimate residue of γ and a suitable partner on α via engineered Cys residues in the region where γ snugly fits into the "hydrophobic bearing" of F_1 (γA285C ↔ αP280C) (19), we hoped to torsionally strain subunit γ upon ATP hydrolysis.

Although the oxidized F_1 carrying similarly engineered cross-links at the center (γL262C ↔ αA334C) or bottom (γCys^{87} ↔ βD380C) positions were hydrolytically inactive (as expected), quantitative disulfide bridge formation at the top position surprisingly did not impede the enzyme function at all, as apparent from both ATP turnover and the rotation assay with a fluorescent actin filament attached to γ (7).

EXPERIMENTAL PROCEDURES

Chemicals and Enzymes—All restriction enzymes were purchased from New England Biolabs (Frankfurt/Main, Germany) or MBI Fermentas (St. Leon-Rot, Germany). Oligonucleotide primers were synthesized by MWG Biotech (Ebersberg, Germany). Ni^{2+}-nitrilotriacetic acid (Ni-NTA)[1] horseradish peroxidase and Ni-NTA superflow were from Qiagen (Hilden, Germany). Biotin-$PEAC_5$-maleimide was from Dojindo (via Gerbu Biotechnik, Gaiberg, Germany). Lumi-light Western blotting kit was obtained from Roche Molecular Biochemicals (Mannheim, Germany). Other reagents were of the highest grade commercially available.

Molecular Genetics—The plasmid pKH7 (all wild-type cysteines substituted by alanines (21), His_6 tag N-terminal at subunit β, γK109C (10)) was used as starting plasmid. For the αP280C, αA334C, γL262C, γA87C (because pKH7 had all endogenous Cys residues substituted for, the wild-type residue γCys^{87} had to be re-introduced), and βD380C mutations, pBluescript II SK (+/−) subclones were generated by insertion of the *Kpn*I/*Xho*I, *Kpn*I/*Sac*I, and *Sac*I/*Xba*I fragments of pKH7. Site-directed mutagenesis was carried out by polymerase chain reaction using the oligonucleotide 5′-GCTGCTCCGTCGTTGTCCAGGACGTGAAG-3′ and its complement 5′-TTATCGAAACTCAGTGTGGTGACGGTCGGTCG-3′ for αP280C, 5′-GAAACGTCACCACACTGAGTTTCGATAATCGG-3′ for αA334C, 5′-TTAAAGAGCTGCAGTGTGTATACAACAAAGATAG-3′ and 5′-CTTTGTATA-CACACTGCAGCTCTTTAATCAG-3′ for γL262C, 5′-CGACCGACCGTGGTTTGTGTGGTGGTTTGAAC-3′ and its complement for γA87C, and 5′-CCATCCTGGGTATGTGT-

[1] The abbreviations used are: Ni-NTA, Ni^{2+}-nitrilotriacetic acid; EF_1, F_1-ATPase from *E. coli*; DTT, dithiothreitol; DTNB, 5,5′-dithiobis-(2-nitrobenzoic acid); Mops, 4-morpholinepropanesulfonic acid; RT, room temperature.

* This work was supported by Deutsche Forschungsgemeinschaft Grant Sonderforschungsbereich 431/D1 (to W. J. and S. E.), a Human Science Frontiers Program grant (to W. J.), and a Humboldt Foundation grant (to D. C.). The costs of publication of this article were defrayed in part by the payment of page charges. This article must therefore be hereby marked "*advertisement*" in accordance with 18 U.S.C. Section 1734 solely to indicate this fact.

‡ To whom correspondence should be addressed. Fax: 49-541-969-2870; E-mail: engel@uos.de.

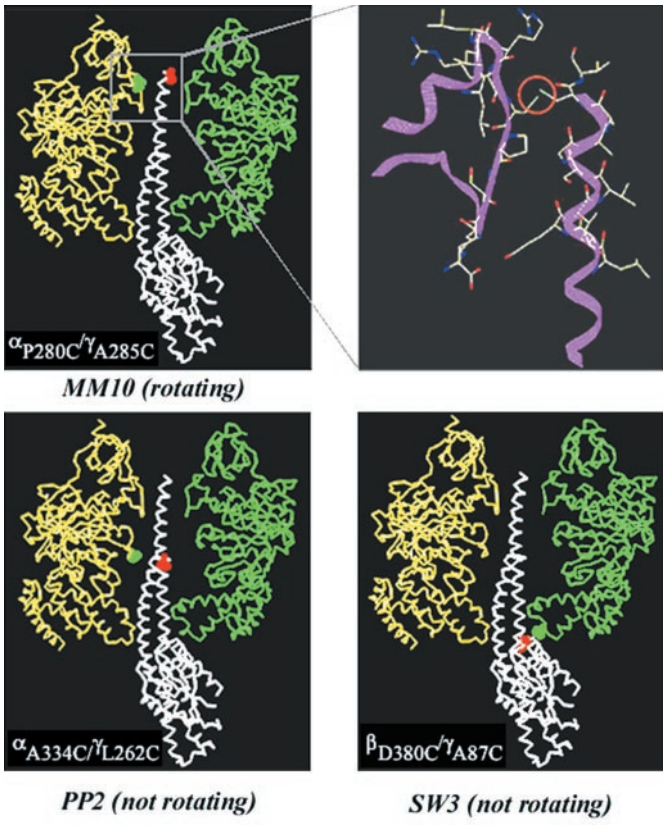

FIG. 1. **Localization of the engineered cysteine residues within EF_1-mutants MM10 (top), PP2 (center), and SW3 (bottom).** The plot was obtained with O (20) by using coordinates from a homology model constructed earlier (16) (*cf.* 131.173.26.96/se/data/ef1/).

GAACTGTCTGAAG-3′ and its complement for βD380C (22). The *Kpn*I/*Sac*I and *Kpn*I/*Xho*I fragments of pKH7 were substituted with the corresponding fragments carrying the γL262C or αP280C mutations by restriction and ligation (resulting in plasmids pBP4 and pMM6, respectively). The αA334C/γL262C double mutant was then generated by exchanging the *Kpn*I/*Xho*I fragment of pBP4 with the corresponding mutated fragment. The γA285C mutant (pMM9) was generated by standard polymerase chain reaction with pKH7 as template and the oligonucleotide primers 5′-GGTACCAATGAGCTCCATCATGTTTA-3′, 5′-CTTCACGTCCTGGACAACGACG-GAGCAAGC-3′, and 5′-CTCGGGG-GCCGCCTGTGTTTAAACAGG-3′ and its complement. The *Kpn*I/*Sac*I fragment of pMM6 was then exchanged against the corresponding fragment containing the γA285C mutation by standard restriction/ligation. The βD380C/γA87C double mutant was generated by substitution of the *Kpn*I/*Xba*I fragment of pKH7 with the *Kpn*I/*Sac*I fragment carrying the γA87C mutation and *Sac*I/*Xba*I fragment of pKG4 carrying the βD380C mutation by triple ligation. Successful cloning was checked by nucleotide sequencing.

The resulting plasmids were pMM10 (αP280C/γA285C), pPP2 (αA334C/γL262C), and pSW3 (βD380C/γA87C).

Preparation of EF_1—Escherichia coli strain DK8 (23) was transformed with the required plasmid, and cells were grown on minimal medium. Cells were collected at A_{600} = 0.8. Membranes were isolated and purified essentially according to Wise (24) except that 5 mM DTT was added to all buffers in the case of PP2. EF_1 was extracted by treatment with 1 mM EDTA in the presence of 1 (MM10, SW3) or 5 (PP2) mM DTT and applied to an anion-exchange column (Tosoh Fractogel TSK-DEAE 650(S), Toyo Soda, Darmstadt, Germany) equilibrated with buffer A (50 mM Tris/H_2SO_4, 1 mM DTT, and 10% (v/v) methanol, pH 7.4). EF_1 was eluted from the column using a stepwise gradient of 0.5 M Na_2SO_4 in buffer A. Enzyme-containing fractions (75–150 mM Na_2SO_4) were combined (yielding 20 mg of protein for MM10 and SW3, 10 mg for PP2 from 12-liter cultures). For further purification aliquots were gel-filtrated through PD-10 columns (Amersham Pharmacia Biotech), which were equilibrated with buffer B (50 mM Tris-HCl, 5 mM $MgCl_2$, 50 mM KCl, 10% (v/v) glycerol, pH 7.5) and then applied to Ni-NTA affinity chromatography (5 mg of protein/ml Ni-NTA-agarose) equilibrated with the same buffer. After washing with buffer B (containing 20 mM imidazole and 1 mM DTT), pure EF_1 was eluted with 150 mM imidazole and 1 mM DTT in buffer B. For cross-linking studies, the eluate was reapplied to a PD-10 gel filtration column equilibrated with buffer B. Protein determination was carried out according to Sedmak and Grossberg (25), resulting in 0.5–1 mg/ml protein, and purity was checked by SDS electrophoresis (Amersham Pharmacia Biotech Phast system, 8–25% gradient gels) without β-mercaptoethanol in the sample buffer. Staining was carried out with Coomassie Silver (26).

Cross-linking of the EF_1 Mutants—Quantitative formation of the cross-link was accomplished by treatment of the enzyme in buffer B with either 100 μM DTNB or 50 μM $CuCl_2$ at ambient temperature for 24 h in the presence of 2 mM ATP. The reactions were quenched with 10 mM *N*-ethylmaleimide and 5 mM EDTA, respectively. The reversibility of the cross-link formation was shown by reduction of the cross-linked product with 50 mM DTT (24 h at RT). All samples were subjected to electrophoresis on a 8–25% SDS-polyacrylamide gel. Gel bands were stained with Coomassie Brilliant Blue R by incubation overnight (27). The gels were scanned and the gel bands were quantified using ImageProPlus 4.0 (Media Cybernetics).

Rotation Assay—Samples were filled into flow cells consisting of two coverslips (bottom, 26 × 76 mm^2; top, 21 × 26 mm^2, thickness 0.15 mm, Menzel-Gläser/ProLabor, Georgsmarienhütte, Germany) separated by parafilm strips. Protein solutions were infused in the following order (2 × 25 μl per step, 4-min incubation): 1) 0.8 μM Ni-NTA-horseradish peroxidase conjugate in 20 mM Mops/KOH (pH 7.0), 50 mM KCl, 5 mM $MgCl_2$ (buffer D); 2) 10 mg/ml bovine serum albumin in buffer D; 3) 5–10 nM EF_1 in buffer D; 4) wash with buffer D; 5) 0.5 μM streptavidin in buffer D; 6) wash with buffer D; 7) 200 nM biotinylated, fluorescently labeled F-actin (14) in buffer D (7-min incubation); 8) wash with buffer D; and 9) 20 mM glucose, 0.2 mg/ml glucose oxidase, 50 μg/ml catalase, and 5 mM ATP in buffer D. Deliberate omission of one single component of the chain Ni-NTA-horseradish peroxidase-biotinylated EF_1-streptavidin-biotin-F-actin prevented the binding of fluorescent F-actin, as evident from the absence of fluorescent filaments within the flow cell. This ensured that the actin filaments were attached to subunit γ in the correct manner.

Because DTNB oxidation caused γCys^{109} to become at least partially blocked and therefore unavailable for the required biotinylation, we used $CuCl_2$ instead. This was followed then by biotinylation with a 20-fold excess of biotin-PEAC5-maleimide for 20 min. Unfortunately, this protocol prevented the immobilization of the enzyme, probably because of competitive binding of Cu^{2+} ions to the His tag. Therefore, the order of steps was reversed. An equimolar amount of biotin-$PEAC_5$-maleimide was used for the biotinylation of nonoxidized MM10 (15 min at RT) at residue γCys^{109} to avoid biotinylation of those cysteines required for cross-link formation. Biotinylated EF_1-MM10 was then oxidized at a protein concentration of 0.5–1 mg/ml in buffer B with 100 μM DTNB in the presence of 2 mM ATP for 24 h followed by PD-10 gel filtration column in buffer B. Completion of cross-link formation (>98%) was confirmed as described above.

Video Microscopy—An inverted fluorescence microscope (IX70, Olympus, lens PlanApo ×100/1.40 oil, fluorescence cube MWIG) was equipped with a silicone-intensified tube camera (C 2400-08, Hamamatsu) and connected to a VHS-PAL video recorder (25 frames/sec). To avoid the reduction of the disulfide bridge in the oxidized samples, the assay was carried out in the absence of β-mercaptoethanol. This resulted in fast bleaching of the fluorescently labeled actin filaments. It was overcome by reducing the excitation intensity to 12% by a neutral density filter (Olympus ND12) and by amplifying the signal by a high performance GEN III intensifier, VideoScope VS4-1845. With this setup filaments 5 μm in length appeared as 3-cm-long rods on a 14-inch monitor. A freshly biotinylated, chromatographed sample of EF_1 was loaded into the flow cell and labeled with fluorescent actin filaments. The rotation of single filaments was observed for up to 3 min. Single molecule rotation was studied up to 30 min after loading. Video data were captured (frame grabber FlashBus, Integral Technologies) and further processed by using the software ImageProPlus 4.0 (Media Cybernetics) and Matlab 5.2 (The Math Works).

Molecular Dynamics Calculations—A three-dimensional model of subunit γ from *E. coli* was constructed by the program X-PLOR (28) from published coordinates of the bovine enzyme (PDB entry 1E1Q). Although the primary structure of γ is not very well conserved (a notable exemption being the C terminus), the matching of the α-helical parts is rather high. The modeled portion of γ comprised the last 30 residues (Ile^{257}-Val^{286}, with Ala^{285} being replaced by Cys) and included the single-helical part of the central shaft and eight residues of the coiled coil. The protein was "solvated" by TIP3 rigid water molecules (29), which formed a cylinder with a diameter of 2.4 nm and height of 7

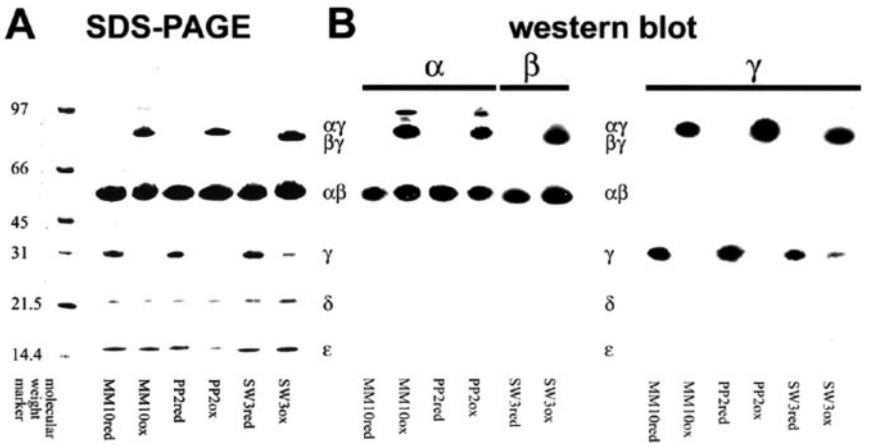

FIG. 2. **SDS-polyacrylamide gel electrophoresis (8–25% Amersham Pharmacia Biotech Phast Gel) and Western blots of EF_1-$MM10_T$, -$PP2_C$, and -$SW3_B$ (0.5–1 mg/ml each, 2 mM ATP) before and after oxidation with 100 μM DTNB for 24 h at RT.** *A*, Coomassie Silver stain; *B*, Western blot with anti-α, anti-β, or anti-γ-IgG.

nm. In total, the system contained 472 protein atoms and 843 water molecules. The molecular dynamics simulations were carried out with the program NAMD2 (30) using the all-atom empirical force field CHARMM22 (31). A cylindrical boundary potential was used to prevent water evaporation. A transversal diffusion of the α-helix was restrained by two parabolic potentials: the first one was applied to the united group of four carbonyl C′ atoms of the residues Glu^{259}-Leu^{262} and restricted the transversal motion of the N terminus, and the second potential acted in similar way on the C terminus (residues Thr^{277}-Val^{280}). The system was equilibrated during 100 psec, and then the rotation of γ was forced by a constant torque applied to the N terminus of the helix. The torque was created by four forces acting on the C_α atoms of Leu^{260}, Gln^{261}, Leu^{262}, and Val^{263}, respectively. The magnitude and direction of the forces were calculated at every step of the molecular dynamics integration (1 femto second) by the Tcl script language (32). As a result, each C_α atom experienced an equal torque of 14 pN·nm, and the total torque matched the average torque exerted upon γ under hydrolyzing conditions (~56 pN·nm). To prevent the free rotation of the α-helix as a whole, the S_γ atom of Cys^{285} and one of the terminal carboxyl oxygen atoms of Val^{286} were fixed at those positions that were obtained by the prior equilibration.

In agreement with the results of Schreiber and Steinhauser (33), we found that the stability of the α-helix was sensitive to the truncation of Coulomb interactions. The treatment of full electrostatics by the multiple time-stepping integration scheme distributed parallel multipole tree algorithm, where the total force acting on each atom is broken into two pieces, a quickly varying local component and a slower long range component (34), improved the stability of the α-helix as compared with the calculations at moderate cutoff values of 10–16 Å (several 300-psec tracks of free motion were compared). In the case of forced motion, however, the secondary structure of the α-helix was unstable even if the distributed parallel multipole tree algorithm was used. Probably the $(\alpha\beta)_3$ hexamer stabilizes the α-helical structure of the C terminus of γ, but we did not follow this effect because consideration of $(\alpha\beta)_3$ increased the size of the system enormously and the computational cost of the simulations as well. Instead, we used the following way to stabilize the α-helical conformation. Generally, the potential energy function in CHARMM22 does not include hydrogen bond interactions, and their effects are described only implicitly through van der Waals and electrostatic interactions. The addition of explicit hydrogen-bond terms to the potential energy function increased the rigidity of the α-helix and prevented its distortion when a torque of 56 pN·nm was applied. Such modification of the potential function affected the activation barriers along the ϕ and ψ coordinates only marginally, because the barriers arose mainly because of the van der Waals repulsion of nonpolar atoms.

Other Methods—ATPase activity was measured at protein concentrations of 10 μg/ml in 50 mM Tris-HCl, pH 8.0, 3 mM $MgCl_2$, and 10 mM sodium-ATP. After incubation for 5 min at 37 °C, the reaction was stopped by the addition of trichloroacetic acid, and the released P_i was determined colorimetrically (35). Western blotting on polyvinylidene difluoride membranes was carried out in the Amersham Pharmacia Biotech PhastSystem. Monoclonal primary antibodies directed against EF_1-α, EF_1-β, and EF_1-γ were used at dilutions of 1:200,000, 1:20,000, and 1:15,000, respectively. A peroxidase-conjugated secondary antibody directed against mouse IgG was used then for visualization by chemiluminescence.

RESULTS AND DISCUSSION

EF_1 mutant KH7 (10) was used as starting material. In this mutant, all wild-type cysteines are substituted by alanines (21), one novel cysteine was introduced in γ (K109C), and each β-subunit carried an engineered His_6 tag at the N terminus. To generate mutants suitable for disulfide bridge formation between subunits γ and α or β, additional cysteine residues were introduced at positions 280 or 334 in α, 285, 262, and 87 in γ (this cysteine is present in wild-type EF_1 but was removed in pKH7), and 380 in β. The αP280C/γA285C mutant was named MM10 (top), the αA334C/γL262C mutant was named PP2 (center), and the βD380C/γA87C mutant was named SW3 (bottom). The latter one is similar to a mutant that was used previously by Cross and co-workers (5).

E. coli strain DK8 after transformation with the three respective plasmids grew as well on succinate as the control (pKH7).[2] After purification, both $EF_1(dithiol)_T$ and $EF_1(dithiol)_B$ had normal hydrolytic activities of 120–140 units/mg, whereas the activity of $EF_1(dithiol)_C$ was 70 units/mg under the same conditions and without noticeable amounts of cross-linked enzyme.

Cross-link Formation—Either $CuCl_2$ (50 μM) or DTNB (100 μM) was used for the oxidation of engineered cysteine residues resulting in $EF_1(disulfide)_{T,\,C,\,B}$. After a 24-h incubation the γ monomer band had disappeared completely, indicating quantitative cross-link formation. $EF_1(disulfide)_C$ formed spontaneously by air oxidation. Fig. 2 confirms the quantitative formation of the α-γ ($EF_1(disulfide)_{T,\,C}$) and β-γ ($EF_1(disulfide)_B$) heterodimers by SDS-polyacrylamide gel electrophoresis and Western blot.

Densitometric quantification of the Coomassie-stained bands revealed yields of >98% with $EF_1(disulfide)_T$ and $EF_1(disulfide)_C$ and ~90% for $EF_1(disulfide)_B$. The control EF_1-KH7 did not show heterodimer formation under oxidizing conditions (data not shown). The disulfide bridges were fully reducible in all three mutants by treatment with 50 mM DTT for 24 h with concurrent reappearance of the ATPase activity.

With EF_1-$MM10_T$ and EF_1-$PP2_C$, we observed another high molecular mass low yield oxidation product caused by the formation of an αα homodimer. To exclude that the desired αγ heterodimer was not formed just during sample preparation for SDS electrophoresis, we oxidized samples followed by reduction

[2] In the following, we will use "disulfide" or "dithiol" for the oxidized and reduced forms of EF_1 prepared from these plasmids with a "T," "C," or "B" subscript designating the location of the cysteines at the top, center, and bottom, respectively.

TABLE I
Effects of disulfide bridge formation on hydrolytic ATPase activity

F-mutant	Cross-link position	ATPase activity			Cross-link yield
		Reduced	Oxidized	Re-reduced	
		U/mg			
KH7		140	nd	nd	
$MM10_T$	α280/γ285	140	140	140	> 98%
$PP2_C$	α334/γ262	70	< 1	70	> 98%
$SW3_B$	β380/γ87	140	10	140	~ 90%

and SDS gel electrophoresis in the absence of β-mercaptoethanol. Less than 2% of cross-linked products were thus obtained (data not shown). This confirmed that the disulfide bridge formation occurred in solution and not during SDS sample preparation.

ATP Hydrolysis Activity of Cross-linked EF_1—Both $EF_1(disulfide)_C$ and $EF_1(disulfide)_B$ lost their ATP hydrolysis activities (Table I) both in accordance with expectations and confirming published data (βD380C ↔ γA87C (5)). Much to our surprise, however, the ATPase activity of $EF_1(disulfide)_T$ remained at ~140 units/mg independently of the redox conditions. Closure of the disulfide bridge between residues α280 and γ285 did not impede ATP hydrolysis at all.

This finding was similar to data obtained previously by Musier and Hammes (36). They observed that chemical β/α-γ cross-linking in chloroplast F_1 (likely involving the penultimate endogenous cysteine residue (37)) had only a minor effect on ATPase activity (7–12% decrease). These data have been taken as an argument against the rotary mechanism of ATP hydrolysis/synthesis (38).

Rotational Activity—For direct visualization of rotation of the γ subunit of $EF_1(disulfide)_T$, the microvideography assay of Noji *et al.* (7) was applied. To selectively modify γCys^{109} an equimolar amount of biotin maleimide was used, because the 20-fold excess usually used also biotinylated cysteines αCys^{280} and γCys^{285}, which were required for the disulfide bridge. Under these conditions the subsequent oxidation with 100 μM DTNB in the presence of 2 mM ATP resulted in an almost quantitative formation of the cross-link (~ 98%) (Fig. 3).

After immobilization on Ni-NTA-coated glass, counterclockwise rotating filaments were detected under hydrolyzing conditions (Fig. 4*A*). Rotation trajectories of actin filaments of various lengths are shown in Fig. 4*B*. Up to 5% of the filaments were rotating. Both the high yield and the generated torque were in the same range as with the non-cross-linked enzyme or the control EF_1-KH7.

The observation of rotating filaments attached to γK109C even under conditions in which γA285C was disulfide-bridged to αP380C called for considerable internal rotational freedom at the C-terminal end of γ, because the ATPase activity under these conditions was indistinguishable from the activity measured with the fully reduced enzyme. Disulfide bond cleavage upon ATP hydrolysis, *i.e.* by the generated torque, could be excluded. First, the binding energy of a single disulfide bond at ~200 kJ/mol exceeds the ATP hydrolysis energy (~50 kJ/mol (18)). Second, the disulfide bridge persisted in the oxidized enzyme even after many rounds of ATP hydrolysis, as seen with samples that were first oxidized, then subjected to the ATP hydrolysis assay, and finally to SDS gel electrophoresis (data not shown). The high torque generated by ATP-hydrolyzing EF_1 apparently was sufficient to uncoil the α-helix and to overcome Ramachandran activation barriers.

Molecular Dynamics Calculations—The C-terminal portion of subunit γ contains three residues with considerable rotational freedom (Gly^{282}-Ala^{283}-Ala^{284}). These residues, which are well conserved, therefore would seem to be prime candidates for partial uncoiling of the α-helix during catalytic turnover. For topological constraints, the rotation of γAla^{1}-Ser^{281} in $EF_1(disulfide)_T$ should twist the stretch γGly^{282}-Ala^{284} around the N-C_α and C_α–C′ bonds (rotation around the Ramachandran angles ϕ and ψ). It is known that the ϕ and ψ rotations are restrained by activation barriers of ~60 kJ/mol, such that only a restricted motion in the Ramachandran phase space was observed by NMR relaxation measurements in the time scale of few hundred picoseconds (42). The torque exerted by hydrolyzing F-ATPase, however, could facilitate ϕ, ψ rotations. We used molecular dynamics simulations to investigate the conformational mobility of γ during catalytic turnover of $EF_1(disulfide)_T$.

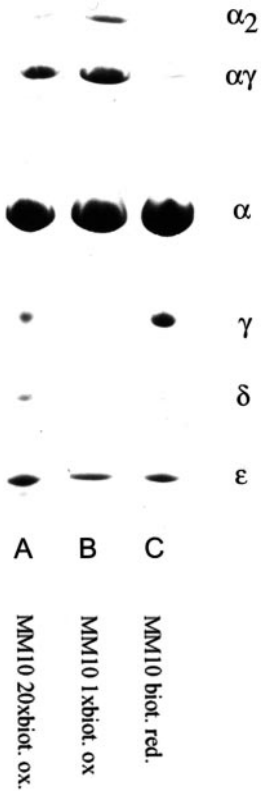

FIG. 3. **SDS-polyacrylamide gel electrophoresis (8–25% Amersham Pharmacia Biotech Phast gel) of biotinylated EF1-MM10T (αP280C/γA285C) after Coomassie staining.** *A*, 20-fold excess biotin maleimide for 20 min at RT, then 100 μM DTNB/2 mM ATP for 24 h at RT. *B*, equimolar amount of biotin maleimide for 15 min at RT, then 100 μM DTNB/2 mM ATP for 24 h at RT. *C*, 50 mM DTT/2 mM ATP for 24 h at RT, then 20-fold excess of biotin maleimide for 20 min at RT.

The rotational dynamics of part of the C-terminal α-helix in subunit γ is shown in Fig. 5 by using the external (θ) and internal (ϕ and ψ) angular coordinates. Fig. 5*A* shows the angular progression of C_α atoms calculated for several selected residues in different positions of the helix. The first 100 psec of the dynamics correspond to the free motion of the system during equilibration. Thereafter a torque of 56 pN·nm was applied to the N terminus. It caused a fast (τ ~ 30 psec) relaxation to a new quasi-equilibrium position caused by elastic deformation of the α-helix. The system rested in this conformation during ~400 psec. After that the helical conformation of the four C-terminal residues Gly^{282}, Ala^{283}, Ala^{284}, and Cys^{285} was lost, and the helix started to rotate. The dynamics of the rotation were nonlinear; it included parts with a high angular velocity of 10^{10} turnovers/sec (such motions were limited apparently by the friction of water) and resting points (where the rotation was temporally blocked by the activation barriers along the internal ϕ, ψ coordinates). The dynamics of coordinates ϕ and ψ calculated for the five C-terminal residues

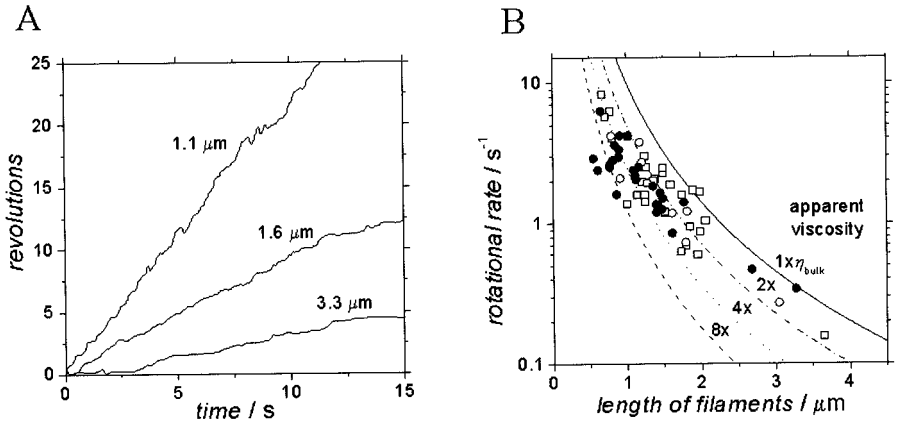

FIG. 4. *A*, three different typical time courses of the rotation of subunit γ. Each *line* represents the counter clockwise rotation of a filament attached to γK109C of EF_1(disulfide)$_T$ in the presence of 5 mM MgATP without the addition of β-mercaptoethanol. *B*, average rotational velocity in revolutions/sec as a function of the length of the actin filaments. *Open/solid symbols* refer to measurements in the presence/absence of β-mercaptoethanol. *Circles* and *squares* show the rotational rates of EF_1-MM10 and KH7, respectively. The *inserted curves* were calculated according to $v = 3T(\ln(L/2r) - 0.447)/(8\pi^2\eta L^3)$ (39), where v is the rate in revolutions/sec, T is 51 pN·nm, the applied torque as calculated from the Gibbs energy of ATP hydrolysis (64 kJ/mol) (18), L is the length of the actin filament, r is 2.8 nm, the radius of the actin filament, and η is the apparent viscosity close to the glass surface, which is enlarged in relationship to the bulk viscosity as indicated ($\eta_{bulk} = 10^{-3}$ Nsm^{-2}) (40, 41). The reasons for the increased surface viscosity (*e.g.* surface obstacles) are treated in more detail in Ref. 18.

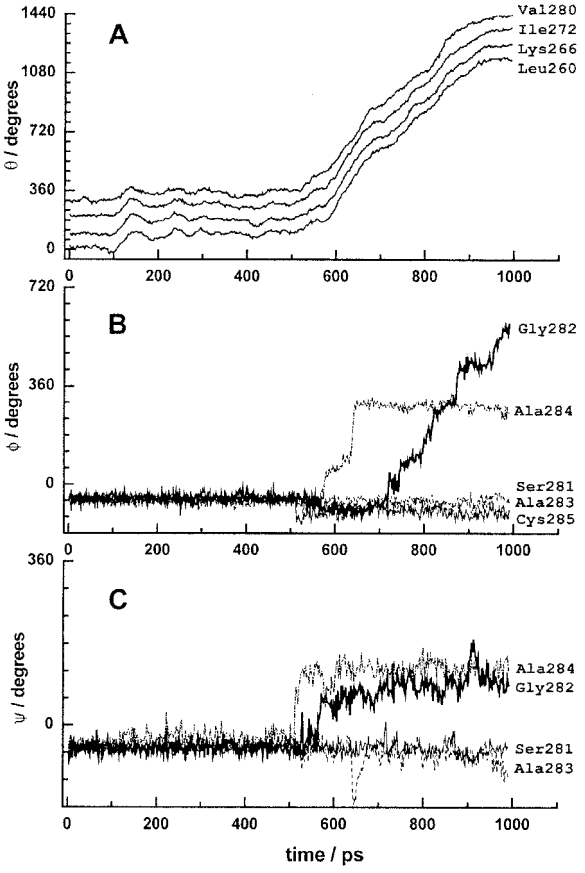

FIG. 5. **Molecular dynamics simulation of the forced rotation of the C-terminal portion of γ.** The first 100 psec corresponded to a free motion of the system (equilibration), and then a constant torque of 56 pN·nm was applied to the N-terminal end of the α-helix. The angular progression of the α-helix was documented by the positions of C_α atoms of four selected residues (*A*) and by the Ramachandran internal angles φ (*B*) and ψ (*C*) calculated for the five C-terminal residues as indicated. Only the conformational changes of Gly^{282} and Ala^{284} residues accounted for the large scale α-helix rotation.

are shown in Fig. 5, *B* and *C*, respectively. These figures demonstrate that only the internal angles of Gly^{282} and Ala^{284} changed essentially during the α-helix rotation. It is worth noting that the initial α-helix unfolding was caused by conformational changes of Ala^{285} (starting at 500 psec), but the later dynamics were mainly caused by the φ rotation of Gly^{282} (starting at 700 psec).

Estimating the heights of the activation barriers along the Ramachandran coordinates yielded values of 25–30 kJ/mol, two times lower than those found by Daragan and Mayo (42). This discrepancy could have arisen from the different methods of calculation. Daragan and Mayo have analyzed the Ramachandran space of rigid molecules (all degrees of freedom were frozen except two selected φ, ψ coordinates). In our case the molecule was free to adopt an optimal configuration, and thus the energy barriers corresponded to the saddle points in the entire multidimensional configuration space of the molecule and thereby are expected to be smaller than the values in a nonequilibrated system.

In summary, we studied the hydrolysis activity and rotation of γ in EF_1 with engineered disulfide bridges between subunits α (belonging to the stator) and γ (rotor) of F_1 at three different positions along the long axis of γ. When the bridge was open, *i.e.* under reducing conditions, both activities were preserved in all three cases. Under oxidizing conditions (bridge closed) they were blocked if the engineered disulfide bridge was positioned at the center or bottom parts of γ. In contrast to the former, the closure of the disulfide bridge at the top position had no effect on the rates of ATP hydrolysis and the rotation of subunit γ.

This result was not likely caused by the forced cleavage of the disulfide bond (strength ~200 kJ/mol) by the rotary motor (free energy of ATP hydrolysis under our conditions ~65 kJ/mol), nor was it caused by a rotation around the disulfide bond (stretching out rather perpendicularly from the rotation axis (compare Fig. 1)). The rotational freedom was likely attributable to the Ramachandran angles φ and ψ of the particularly "bendable" residues, perhaps γGly^{282}-Ala^{283}-Ala^{284} preceding the penultimate and disulfide-bridged γCys^{285}. φ and ψ rotations are restrained by activation barriers of <60 kJ/mol such that only a restricted motion in the Ramachandran phase space was observed by NMR relaxation measurements on a time scale of few hundred picoseconds. Our data give evidence that the high torque generated by ATP hydrolysis by EF_1 is sufficient to uncoil an α-helix and to overcome Ramachandran activation barriers.

The completely unaffected activities of EF_1(disulfide)$_T$ in comparison with EF_1(dithiol)$_T$ or EF_1-KH7, ATP hydrolytic activity, and rotation along with the results of the molecular

dynamics calculations are suggestive of the conserved γGly^{282}-Ala^{283}-Ala^{284} serving even in the wild-type enzyme as a physiological swivel point. In other words, the top part of γ might be tethered permanently to $(\alpha\beta)_3$. This is currently under investigation.

Acknowledgments—Skillful technical assistance by Gabriele Hikade and Hella Kenneweg is gratefully acknowledged. The monoclonal antibodies used in this study were a kind gift of Dr. G. Deckers-Hebestreit (Department of Microbiology, University of Osnabrück, Germany).

REFERENCES

1. Boyer, P. D. (1997) *Annu. Rev. Biochem.* **66,** 717–749
2. Junge, W., Lill, H., and Engelbrecht, S. (1997) *Trends Biochem. Sci.* **22,** 420–423
3. Fillingame, R. H. (2000) *Nat. Struct. Biol.* **7,** 1002–1004
4. Jiang, W., Hermolin, J., and Fillingame, R. H. (2001) *Proc. Natl. Acad. Sci. U. S. A.* **98,** 4966–4971
5. Duncan, T. M., Bulygin, V. V., Zhou, Y., Hutcheon, M. L., and Cross, R. L. (1995) *Proc. Natl. Acad. Sci. U. S. A.* **92,** 10964–10968
6. Sabbert, D., Engelbrecht, S., and Junge, W. (1996) *Nature* **381,** 623–626
7. Noji, H., Yasuda, R., Yoshida, M., and Kinosita, K. (1997) *Nature* **386,** 299–302
8. Katoyamada, Y., Noji, H., Yasuda, R., Kinosita, K., and Yoshida, M. (1998) *J. Biol. Chem.* **273,** 19375–19377
9. Omote, H., Sambonmatsu, N., Saito, K., Sambongi, Y., Iwamoto-Kihara, A., Yanagida, T., Wada, Y., and Futai, M. (1999) *Proc. Natl. Acad. Sci. U. S. A.* **96,** 7780–7784
10. Noji, H., Häsler, K., Junge, W., Kinosita, K., Jr., Yoshida, M., and Engelbrecht, S. (1999) *Biochem. Biophys. Res. Commun.* **260,** 597–599
11. Hisabori, T., Kondoh, A., and Yoshida, M. (1999) *FEBS Lett.* **463,** 35–38
12. Zhou, Y. T., Duncan, T. M., Bulygin, V. V., Hutcheon, M. L., and Cross, R. L. (1996) *Biochim. Biophys. Acta* **1275,** 96–100
13. Sambongi, Y., Iko, Y., Tanabe, M., Omote, H., Iwamoto-Kihara, A., Ueda, I., Yanagida, T., Wada, Y., and Futai, M. (1999) *Science* **286,** 1722–1724
14. Pänke, O., Gumbiowski, K., Junge, W., and Engelbrecht, S. (2000) *FEBS Lett.* **472,** 34–38
15. Tsunoda, S. P., Aggeler, R., Yoshida, M., and Capaldi, R. A. (2001) *Proc. Natl. Acad. Sci. U. S. A.* **98,** 898–902
16. Engelbrecht, S., and Junge, W. (1997) *FEBS Lett.* **414,** 485–491
17. Cherepanov, D. A., and Junge, W. (2001) *Biophys. J.* **81,** 1234–1244
18. Pänke, O., Cherepanov, D. A., Gumbiowski, K., Engelbrecht, S., and Junge, W. (2001) *Biophys. J.* **81,** 1220–1233
19. Abrahams, J. P., Leslie, A. G. W., Lutter, R., and Walker, J. E. (1994) *Nature* **370,** 621–628
20. Jones, T. A., Zou, J. Y., Cowan, S. W., and Kjeldgaard, M. (1991) *Acta Crystallogr. A* **47,** 110–119
21. Kuo, P. H., Ketchum, C. J., and Nakamoto, R. K. (1998) *FEBS Lett.* **426,** 217–220
22. Weiner, M. P., Costa, G. L., Schoettlin, W., Cline, J., Mathur, E., and Bauer, J. C. (1994) *Gene* (*Amst.*) **151,** 119–123
23. Klionsky, D. J., Brusilow, W. S. A., and Simoni, R. D. (1984) *J. Bacteriol.* **160,** 1055–1060
24. Wise, J. G. (1990) *J. Biol. Chem.* **265,** 10403–10409
25. Sedmak, J. J., and Grossberg, S. E. (1994) *Anal. Biochem.* **79,** 544–552
26. Krause, I., and Elbertzhagen, H. (1987) in *A 5 Minute Silver Stain for Dried Polyacrylamide Gels* (In Radola, B. J., ed) Elektrophoreseforum, TU München, Germany (in German)
27. Downer, N. W., and Robinson, N. C. (1976) *Biochemistry* **15,** 2930–2936
28. Brünger, A. T. (1992) *X-PLOR*, Version 3.1, Yale University Press, New Haven, CT
29. Jorgenson, W. L., Chandrasekhar, J., and Madura, J. D. (1983) *J. Chem. Phys.* **79,** 926–935
30. Kale, L., Skeel, R., Bhandarkar, M., Brunner, R., Gursoy, A., Krawetz, N., Phillips, J., Shinozaki, A., Varadarajan, K., and Schulten, K. (1999) *J. Comp. Phys.* **151,** 283–312
31. Brooks, B. R., Bruccolori, R. E., Olafson, B. D., States, D. J., Swaminathan, S., and Karplus, M. (1983) *J. Comput. Chem.* **4,** 187–217
32. Dalke, A., and Schulten, K. (1997) *Pac. Symp. Biocomput.* 85–96
33. Schreiber, H., and Steinhauser, O. (1992) *Biochemistry* **31,** 5856–5860
34. Rankin, W., and Board, J. A (2001) *Portable Distributed Implementation of the Parallel Multipole Tree Algerithm*, Institute of Electrical and Electronic Engineers Symposium on High Performance Distributed Computing, Duke University Technical Report 95-002, in press
35. LeBel, D., Poirier, G. G., and Beaudoin, A. R. (1978) *Anal. Biochem.* **85,** 86–89
36. Musier, K. M., and Hammes, G. G. (1987) *Biochemistry* **26,** 5982–5988
37. Moroney, J. V., Fullmer, C. S., and McCarty, R. E. (1984) *J. Biol. Chem.* **259,** 7281–7285
38. McCarty, R. E., and Evron, Y. (2000) *Annu. Rev. Plant. Physiol. Plant Mol. Biol.* **51,** 83–109
39. Hunt, A. J., Gittes, F., and Howard, J. (1994) *Biophys. J.* **67,** 766–781
40. Yasuda, R., Noji, H., Yoshida, M., Kinosita, K., Jr., and Itoh, H. (2001) *Nature* **410,** 898–904
41. Yasuda, R., Noji, H., Kinosita, K., and Yoshida, M. (1998) *Cell* **93,** 1117–1124
42. Daragan, V. A., and Mayo, K. H. (1993) *Biochemistry* **32,** 11488–11499